Three-Dimensional Covalent Organic Frameworks with scu Topology

Saikat Das,† Taishu Sekine,† Haruna Mabuchi,† Tsukasa Irie,† Jin Sakai,† and Yuichi Negishi†,*

†Department of Applied Chemistry, Faculty of Science, Tokyo University of Science, Kagurazaka, Shinjuku-ku, Tokyo 162-8601, Japan

KEYWORDS: covalent organic framework; topology; drug delivery

ABSTRACT: Three-dimensional (3D) covalent organic frameworks (COFs) exemplify a new generation of crystalline extended solids with intriguing structures and unprecedented porosity. Notwithstanding substantial scope, the reticular synthesis of 3D COFs from pre-designed building units leading to new network topologies yet remains a demanding task owing to the shortage of 3D building units and inadequate reversibility of the linkages between the building units. In this work, by linking a tetragonal prism (8-connected) node with a square planar (4-connected) node, we report the first 3D COF with **scu** topology. The new COF, namely TUS-84, features a two-fold interpenetrated structure with well-defined porosity and a Brunauer–Emmett–Teller surface area of 679 $m^2 g^{-1}$. In drug delivery applications, TUS-84 shows efficient drug loading and sustained release profile.

An emerging class of porous organic materials developed from linking molecular building blocks with strong covalent bonds into crystalline, extended (two-dimensional) 2D and (three-dimensional) 3D structures called covalent organic frameworks (COFs)[1-14] have recently aroused great interest in catalysis[15,16], sensing[17,18], separation,[19] semiconduction,[20] proton conduction,[21] biomedicine[22,23], among others. COFs emerged in 2005[24] as the second series of reticular materials, the first one being metal-organic frameworks (MOFs)[25,26]. 'Reticular' means 'anything that has the structure of a net'. By reticular synthesis, we refer to the extended structure regime that combines (*i*) molecular-level control over matter and (*ii*) robustness.[27-29] A top-down reticular synthesis scheme starts with a desired net topology followed by disassembling it into vertices and edges, finding secondary building units with the right connectivities and aligning them with the vertices, obtaining an augmented net by replacing the vertices of an *n*-connected net by a group of *n*-vertices, and finally linking the molecular building blocks by robust bonds into crystalline extended structures.[1,30-34] Alternatively, the bottom-up scheme of reticular synthesis proceeds from pre-designed building units leading to unprecedented network topologies.[35] COFs feature one of the highest open-pore scaffolds. The COF scaffold is built out of organic units and it imparts tunable chemical environments for encapsulating a wide array of guest molecules.

Based on the extension of their covalent connectivity, COFs can be categorized into 2D and 3D COFs.[36] With covalent connectivity extending only in 2D, 2D COFs crystallize as layered structures in which the layers are stacked through non-covalent interactions (π–π stack, Van der Waals interactions, hydrogen bonds), giving rise to 1D straight channels.[14,37] On the other hand, with covalent connectivity extending along the entire 3D scaffold, 3D COFs often have the upper hand over 2D COFs, attributed to their interconnected channels and readily accessible active sites.[38]

Topological consideration is crucial to 3D extended structures considering that it largely dictates their pore architecture, active site formation and mass transport behavior.[38] Albeit highly sought after, discovery of new 3D COF topologies yet remains a herculean task because the highly-connected 3D organic building blocks are hard to come by and it is very difficult to solve the crystal structures. Thus far, the type of 3D topologies of COFs is limited to about 20.[38] The tetratopic (T_d)-based 3D COF nets are **bor**,[39] **ctn**,[39] **dia**,[40] **pts**,[41] **rra**,[42] **lon**,[43] and **ljh**[44]. Fang et al. and He et al. prepared several hexatopic (D_{3h})-based 3D COFs e.g. **stp**,[45] **acs**,[46,47] **ceq**,[47,48] and **hea**[49,50]. Different from triangular prismatic (D_{3h}) nodes, Mateo-Alonso et al. utilized triangular antiprismatic (D_{3d}) nodes to construct **pcu** topology 3D COFs.[51] Other unprecedented 3D COF topologies reported are **ffc**,[52] **srs**,[53] **fjh**,[54] **tbo**,[55] and **nbo**[56]. Recently, octatopic nodes have been used to prepare **pcb**[57] and **bcu**[58] topology 3D COFs.

Herein, we report for the first time a novel 3D COF, namely TUS-84, with **scu** topology formed though the combination of a tetragonal prism (8-connected) node with a square

Scheme 1. Strategy for Constructing 3D COF with the scu Topology[a]

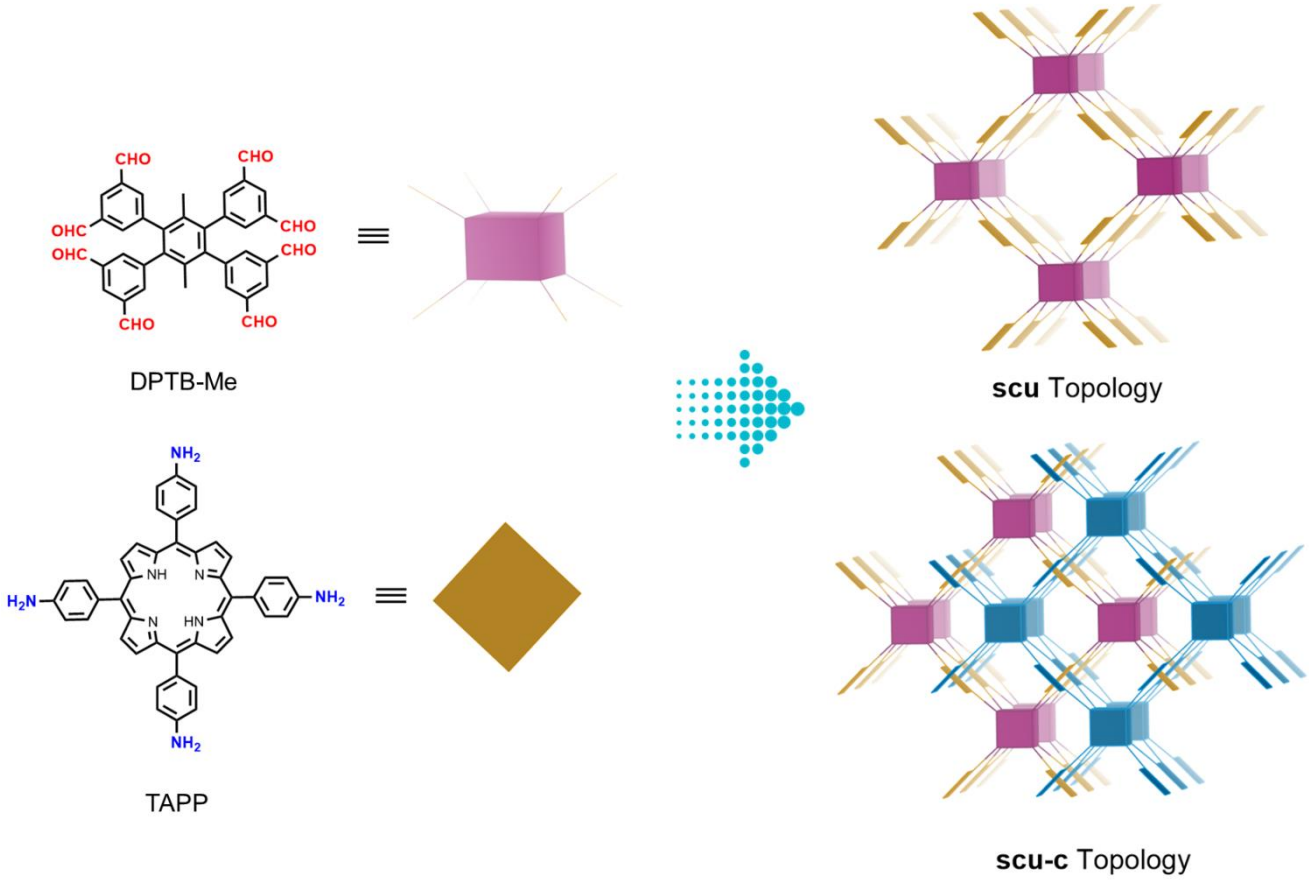

[a]The condensation reaction of a D_{2h}-symmetric linker, DPTB-Me, and a C_4-symmetric linker, TAPP, yielding 3D COF with a **scu-c** net, which belongs to **scu** topology.

planar (4-connected) node. TUS-84 exhibits a two-fold interpenetrated **scu** net, denoted as **scu-c** (c for catenated), with permanent porosity and a Brunauer–Emmett–Teller (BET) surface area of 679 $m^2\ g^{-1}$. Structural elucidation of the COF was carried out thoroughly through different characterization techniques. Interestingly, the COF shows efficient drug loading and extended-release profile in simulated physiological media. Scheme 1 depicts the strategic approach to construct 3D COFs with **scu-c** net via the [8+4] imine condensation reaction of a D_{2h}-symmetric linker, 4',5'-bis(3,5-diformylphenyl)-3',6'-dimethyl-[1,1':2',1''-terphenyl]-3,3'',5,5''-tetracarbaldehyde (DPTB-Me), and a C_4-symmetric linker, 5,10,15,20-tetrakis(4-aminophenyl)porphyrin (TAPP).

TUS-84 was synthesized by the solvothermal reaction of DPTB-Me (19.0 mg, 0.03 mmol) and TAPP (40.48 mg, 0.06 mmol) in a 5:5:2 (v/v/v) mixture of mesitylene, 1,4-dioxane, and 6 M aqueous acetic acid under 120 °C for 3 days. The acid-catalyzed Schiff-base condensation reaction yielded the COF as a dark purple crystalline solid at a yield of 76%. The solid-state ^{13}C cross-polarization magic angle spinning (CP/MAS) NMR and Fourier-transform infra-red (FT-IR) spectroscopies provided definitive evidence for atomic-level connectivity of the imine linkage in TUS-84. The ^{13}C CP/MAS NMR spectrum displayed a characteristic peak at 158 ppm for the imine carbon of TUS-84 (Figure S1). In the FT-IR spectrum of TUS-84, the C=N vibration peak at 1625 cm^{-1} was observed. Significant attenuation of the N-H (3433, 3465 cm^{-1} for TAPP) and C=O (1703 cm^{-1} for DPTB-Me) stretching vibration bands in the FT-IR spectrum of TUS-84 implies high degree of polymerization for the imine COF (Figure S2). Isometric microcrystals of TUS-84 were observed from scanning electron micrographs (Figure S3). High-resolution transmission electron microscopy (HRTEM) imaging (Figure 1b,c, S4,5) showed the ordered structure of TUS-84, comprising rhombus pores viewed along the *z*-direction in the simulated structure (Figure 2a). Thermogravimetric analysis (TGA) curve indicates high thermal stability for TUS-84 retaining 95% of its weight up to 500 °C (Figure S6). Chemical stability of the COF was substantiated from its preservation of crystallinity and imine linkage after treatment with organic solvents, water, and aqueous HCl and NaOH solutions, as can be seen from the PXRD profiles (Figure S7) and FT-IR spectra (Figure S8).

The crystal structure of TUS-84 was unraveled by powder X-ray diffraction (PXRD) analysis combined with structural modeling and simulation (Figure 1a). Geometry optimization (energy minimization) was performed in *Materials Studio* 7.0[59] Forcite program that afforded the unit cell parameters of TUS-84 with a **scu-c** net and *Pm* space group as a = 39.9205 Å, b = 18.7162 Å, c = 23.6564 Å, $\alpha = \beta = \gamma =$

90°. The simulated PXRD pattern (Figure 1a, green curve) showed great alignment with the observed diffraction pattern (Figure 1a, red dots). Sharp Bragg peaks observed at 4.38 and 6.44° correspond to the (200) and (111) facets, respectively and relatively weak peaks at 9.10, 10.23, 11.15, 12.83, 14.38 and 16.19° correspond to the (112), (020), (221), (222) (130) and (132) facets, respectively (Figure 1a). Pawley refinement was applied against the experimental PXRD data using Reflex that resulted in a space group of *Pm* with unit cell parameters a = 39.9179 Å, b = 18.7054 Å, c = 23.6772 Å, $\alpha = \beta = \gamma = 90°$ and good agreement factors R_p = 4.37%, R_{wp} = 3.19%. The Pawley refined PXRD pattern (black curve, Figure 1a) shows good consistency with the experimental PXRD pattern (red dots), as indicated by the minor difference plot (blue curve). Furthermore, we also explored alternative topologies for TUS-84, including the non-interpenetrated **scu** net (Figure S16, Table S2), and **csq** topology (Figure S17, Table S3). However, the simulated PXRD patterns did not accord with the experimental PXRD pattern. All things considered, we propose the **scu-c** net for TUS-84.

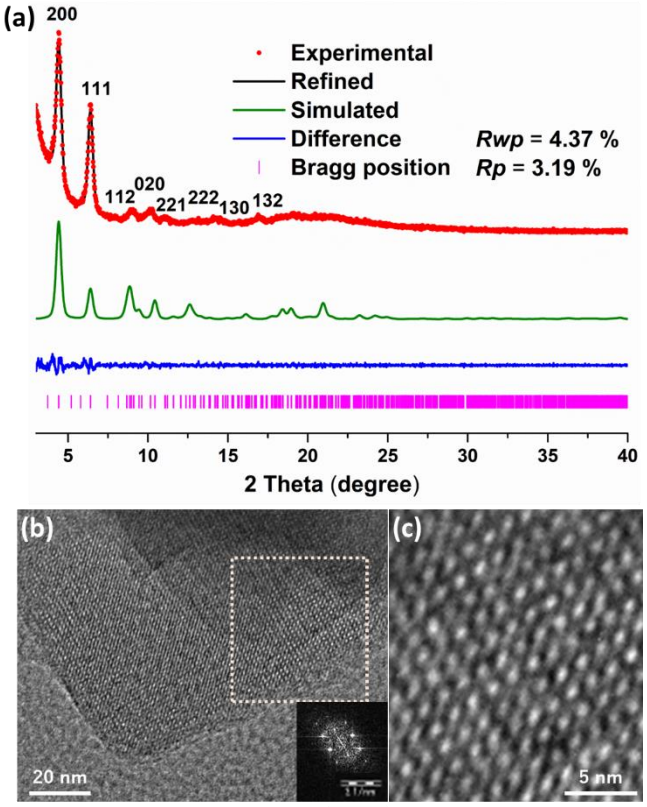

Figure 1. (a) PXRD patterns of TUS-84: experimental pattern (red dots), Pawley refined (black curve), simulated (green curve) pattern from the **scu-c** modeled structure, and the difference plot (blue curve) between the experimental and refined patterns. The Bragg positions are denoted by magenta ticks. (b,c) HRTEM images of TUS-84. Inset in Figure b shows the fast Fourier transform (FFT) pattern acquired from the area enclosed by the white box.

The permanent porosity of TUS-84 was ascertained by N_2 sorption measurements on activated COF sample at 77 K. As can be observed in Figure 3a, TUS-84 displayed a reversible type-I isotherm with a sharp uptake at low pres

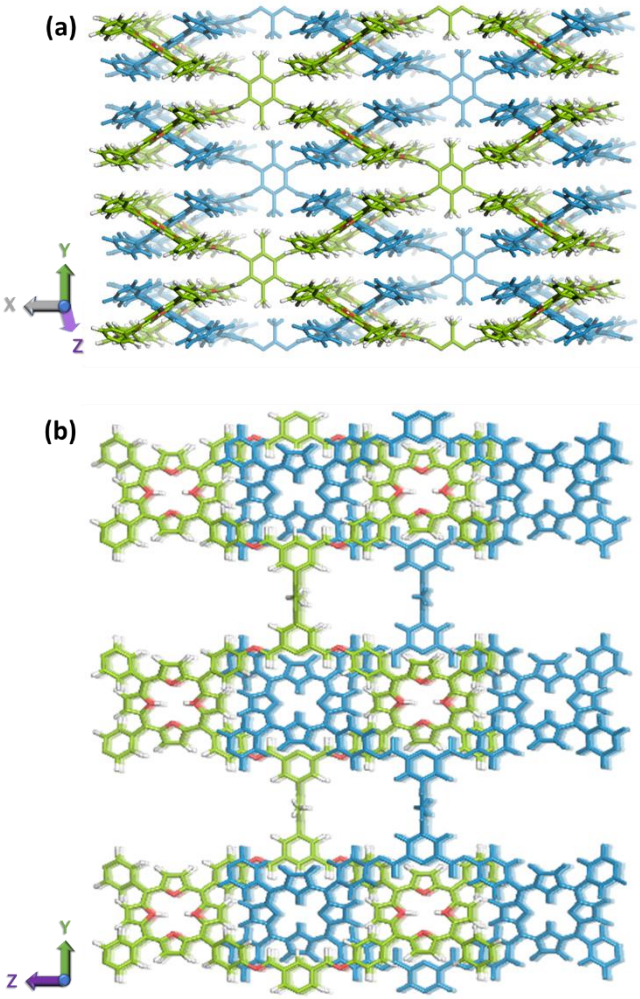

Figure 2. Extended structures of TUS-84.

sure (P/P_0 < 0.1), indicative of its microporous character. The BET specific surface area of TUS-84 was evaluated as 679 $m^2\ g^{-1}$ (Figure S9). Applying the nonlocal density functional theory (NLDFT) method, the pore volume of TUS-84 was derived as 0.7613 $cm^3\ g^{-1}$ and its pore size distribution was calculated as 0.97 nm (Figure 3b), consistent with the pore size predicted from the simulated structure (1.05 nm). We also evaluated the H_2, CO_2 and CH_4 gas adsorption capacities of TUS-84 to reinforce its prospects in carbon capture and clean energy applications. As illustrated in Figure S10, the H_2 uptake capacities at 77 and 87 K under 1 bar are 131 $cm^3\ g^{-1}$ and 88 $cm^3\ g^{-1}$, respectively. The isosteric enthalpy of adsorption (Q_{st}) of H_2 was calculated to be 6.8 kJ mol^{-1} (Figure S11). TUS-84 shows a CO_2 uptake capacity of 55 $cm^3\ g^{-1}$ and 31 $cm^3\ g^{-1}$ at 273 and 298 K, respectively, under 1 bar (Figure S12). The Q_{st} of CO_2 adsorption was evaluated as 24.9 kJ mol^{-1} (Figure S13). The CH_4 sorption isotherms shown in Figure S14 reveal an uptake capacity of 14 $cm^3\ g^{-1}$ and 10 $cm^3\ g^{-1}$ at 273 and 298 K under 1 bar, respectively, and the value of Q_{st} was obtained as 6.5 kJ mol^{-1} (Figure S15).

Intrigued by the 3D functional scaffold with permanent porosity and high chemical stability, we utilized TUS-84 in *in vitro* drug delivery studies. Ibuprofen is one of the most common nonsteroidal anti-inflammatory drugs (NSAIDs)

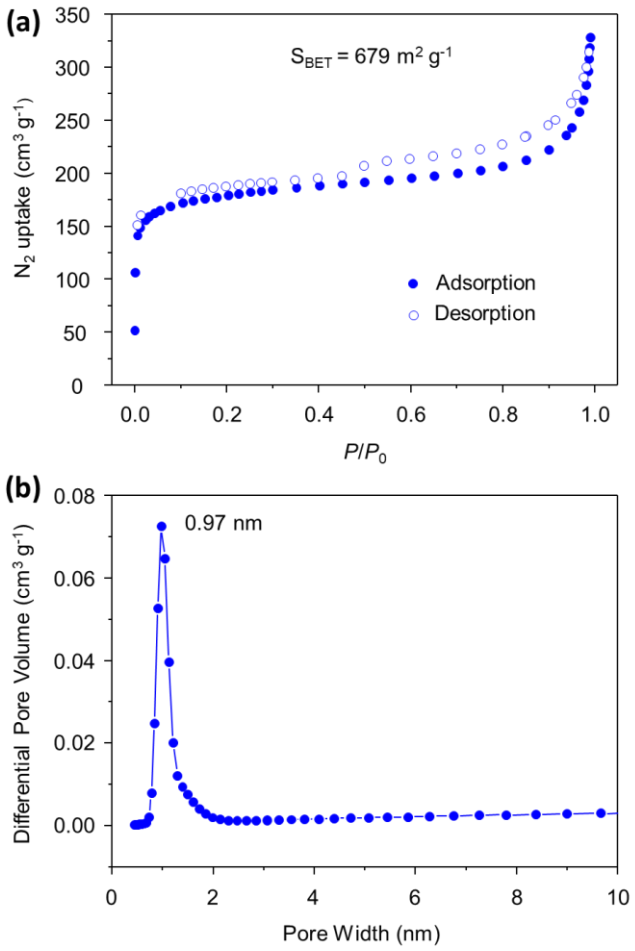

Figure 3. (a) Nitrogen sorption isotherms and (b) pore size distribution profile of TUS-84.

used for the treatment of rheumatoid arthritis, osteoarthritis, mild–moderate pain and primary dysmenorrhea.[60-62] The selection of ibuprofen as the drug in this study is based on: (a) ibuprofen has short half-life (1.8-2.0 h) that calls for extended-release formulations,[1] and (b) pore dimensions of TUS-84 (1.05 nm) is befitting for encapsulation of ibuprofen with molecular size of 0.5 × 1 nm[2,63,64]

For drug loading, 50 mg of TUS-84 was suspended in 30 mL of 0.1 M hexane solution of ibuprofen under magnetic stirring for 5 h. The drug-loaded COF sample was isolated from suspension via vacuum filtration, washed with hexane, and subsequently dried at room temperature. 1.0 mL of the filtrate was collected and 50 times diluted to evaluate the loading amount of ibuprofen using a UV-Vis spectrophotometer by measuring the absorbance at 261 nm of ibuprofen in hexane and supernatant (see SI for details). UV-Vis absorption data showed 11.05 wt% loading of ibuprofen in TUS-84 (Figure S23). As can be seen from Figure S21, the value of drug loading amount is in good agreement with that obtained from the TGA (11 wt%). PXRD analysis (Figure S18) and scanning electron micrograph (Figure S19) of ibuprofen-loaded TUS-84 revealed that the COF crystalline structure was retained after drug loading. The drug release study was performed by placing 40 mg of the drug-loaded TUS-84 sample inside a semipermeable

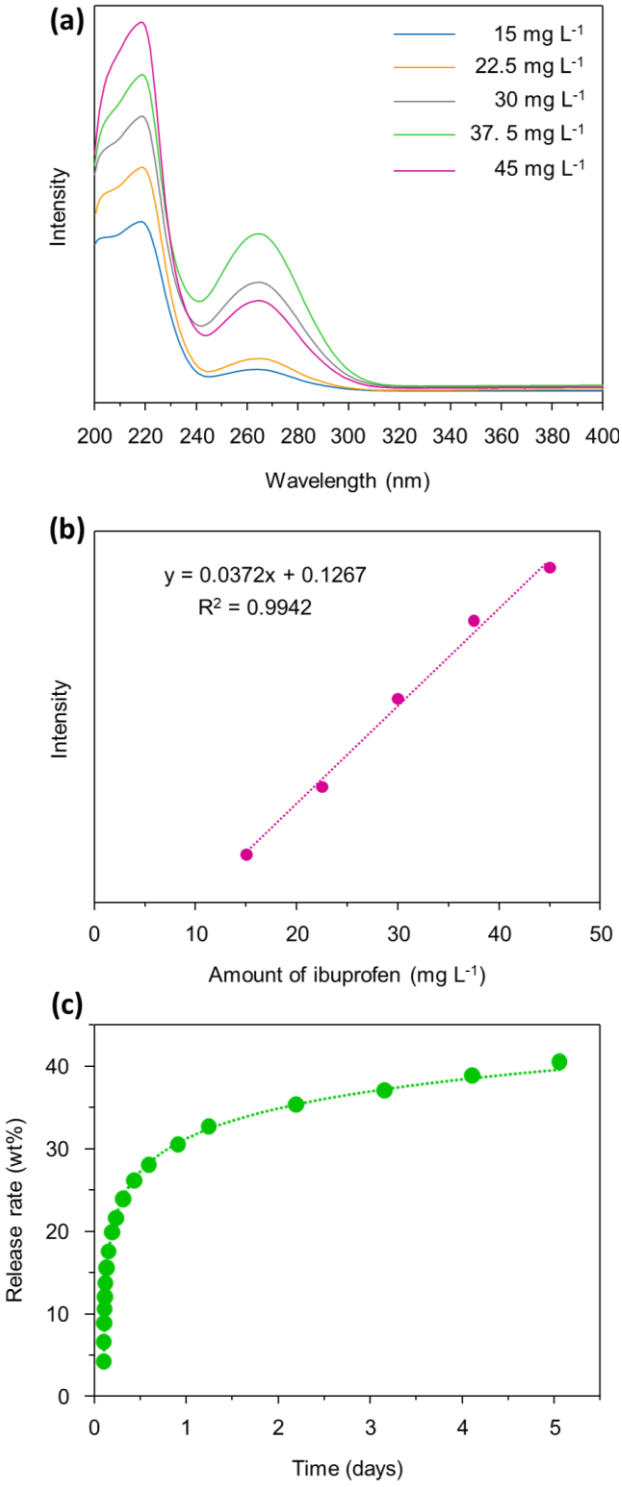

Figure 4. (a) UV-Vis spectra of ibuprofen in simulated body fluid (pH 7.4, phosphate buffer solution) at different concentrations. (b) Calibration curve of ibuprofen. (c) Release profile of ibuprofen from ibuprofen-loaded TUS-84 and corresponding fitting curve.

bag followed by immersing in 10 mL of phosphate buffer solution (simulated body fluid, pH 7.4) at a constant temperature of 37 °C. The dissolution solvent was taken out at specified time intervals for evaluation of the ibuprofen concentration and replenished with 10 mL of fresh buffer

solution. The ibuprofen concentration was determined UV-Vis spectrophotometrically using calibration curve (Figure 4a,b). TUS-84 showed an extended drug release performance of about 40% after 5 days (Figure 4c). This long-acting ibuprofen formulation could deliver sustained concentrations of drug over a prolonged period of time, thereby reducing dosing frequency and ensuring more consistent control of long-lasting pains.[65,66]

To conclude, a 3D COF with a novel **scu-c** topology was designed and synthesized, utilizing a D_{2h}-symmetric linker, DPTB-Me, and a C_4-symmetric linker, TAPP. The resultant TUS-84 COF displays an ordered microporous structure with high crystallinity and excellent stability. Furthermore, TUS-84 shows great promise as drug delivery vehicle owing to its efficient drug loading and controlled release behavior. This study may not only expand the library of 3D COF topologies but also facilitate the design of new 3D COF structures for biomedical applications.

ASSOCIATED CONTENT

Supporting Information.
Materials and characterization; Synthetic procedures; Solid-state ^{13}C CP/MAS Nuclear Magnetic Resonance (NMR) spectroscopy; Fourier-Transform Infrared (FT-IR) spectroscopy; Scanning electron microscopy (SEM) and transmission electron microscopy (TEM) images; Thermogravimetric analysis (TGA); Chemical stability test; N_2 adsorption; Structure simulations and X-ray diffraction analyses; Crystallographic information.
This material is available free of charge via the Internet at http://pubs.acs.org.

AUTHOR INFORMATION

Corresponding Authors

*__Yuichi Negishi__ – Email: negishi@rs.tus.ac.jp

Notes

The authors declare no competing financial interest.

ACKNOWLEDGMENT

This work was supported by the Japan Society for the Promotion of Science (JSPS) KAKENHI (grant numbers 20H02698 and 20H02552), and Scientific Research on Innovative Areas “Aquatic Functional Materials” (grant number 22H04562). Funding provided by the Yazaki Memorial Foundation for Science and Technology, and the Ogasawara Foundation for the Promotion of Science and Engineering is also gratefully acknowledged.

REFERENCES

(1) Diercks, C. S.; Yaghi, O. M. The atom, the molecule, and the covalent organic framework. *Science* **2017**, *355*, eaal1585.

(2) Geng, K.; He, T.; Liu, R.; Dalapati, S.; Tan, K. T.; Li, Z.; Tao, S.; Gong, Y.; Jiang, Q.; Jiang, D. Covalent Organic Frameworks: Design, Synthesis, and Functions. *Chem. Rev.* **2020**, *120*, 8814–8933.

(3) Colson, J.; Dichtel, W. Rationally synthesized two-dimensional polymers. *Nature Chem.* **2013**, *5*, 453–465.

(4) Haase, F.; Lotsch, B. V. Solving the COF trilemma: towards crystalline, stable and functional covalent organic frameworks. *Chem. Soc. Rev.* **2020**, *49*, 8469–8500.

(5) Lohse, M. S.; Bein, T. Covalent Organic Frameworks: Structures, Synthesis, and Applications. *Adv. Funct. Mater.* **2018**, *28*, 1705553.

(6) Zhao, X.; Pachfule, P.; Thomas, A. Covalent organic frameworks (COFs) for electrochemical applications. *Chem. Soc. Rev.* **2021**, *50*, 6871–6913.

(7) Ding, S.-Y.; Wang, W. Covalent organic frameworks (COFs): from design to applications. *Chem. Soc. Rev.* **2013**, *42*, 548–568.

(8) Han, X.; Yuan, C.; Hou, B.; Liu, L.; Li, H.; Liu, Y.; Cui, Y. Chiral covalent organic frameworks: design, synthesis and property. *Chem. Soc. Rev.* **2020**, *49*, 6248–6272.

(9) Kandambeth, S.; Dey, K.; Banerjee, R. Covalent Organic Frameworks: Chemistry beyond the Structure. *J. Am. Chem. Soc.* **2019**, *141*, 1807–1822.

(10) Song, Y.; Sun, Q.; Aguila, B.; Ma, S. Opportunities of Covalent Organic Frameworks for Advanced Applications. *Adv. Sci.* **2019**, *6*, 1801410.

(11) Li, X.; Yadav, P.; Loh, K. P. Function-oriented synthesis of two-dimensional (2D) covalent organic frameworks – from 3D solids to 2D sheets. *Chem. Soc. Rev.* **2020**, *49*, 4835–4866.

(12) Segura, J. L.; Mancheño, M. J.; Zamora, F. Covalent organic frameworks based on Schiff-base chemistry: synthesis, properties and potential applications. *Chem. Soc. Rev.* **2016**, *45*, 5635–5671.

(13) Li, Y.; Chen, W.; Xing, G.; Jiang, D.; Chen, L. New synthetic strategies toward covalent organic frameworks. *Chem. Soc. Rev.* **2020**, *49*, 2852–2868.

(14) Guan, X.; Chen, F.; Fang, Q.; Qiu, S. Design and applications of three dimensional covalent organic frameworks. *Chem. Soc. Rev.* **2020**, *49*, 1357–1384.

(15) Ding, S. Y.; Gao, J.; Wang, Q.; Zhang, Y.; Song, W. G.; Su, C. Y.; Wang, W. Construction of covalent organic framework for catalysis: Pd/COF-LZU1 in Suzuki-Miyaura coupling reaction. *J. Am. Chem. Soc*. **2011**, *133*, 19816–19822.

(16) Xu, H.; Gao, J.; Jiang, D. Stable, crystalline, porous, covalent organic frameworks as a platform for chiral organocatalysts. *Nat. Chem.* **2015**, *7*, 905–912.

(17) Peng, Y.; Huang, Y.; Zhu, Y.; Chen, B.; Wang, L.; Lai, Z.; Zhang, Z.; Zhao, M.; Tan, C.; Yang, N.; Shao, F.; Han, Y.; Zhang, H. Ultrathin Two-Dimensional Covalent Organic Framework Nanosheets: Preparation and Application in Highly Sensitive and Selective DNA Detection. *J. Am. Chem. Soc.* **2017**, *139*, 8698–8704.

(18) Wu, X.; Han, X.; Xu, Q.; Liu, Y.; Yuan, C.; Yang, S.; Liu, Y.; Jiang, J.; Cui, Y. Chiral BINOL-Based Covalent Organic Frameworks for Enantioselective Sensing. *J. Am. Chem. Soc.* **2019**, *141*, 7081–7089.

(19) Huang, N.; Krishna, R.; Jiang, D. Tailor-Made Pore Surface Engineering in Covalent Organic Frameworks: Systematic Functionalization for Performance Screening. *J. Am. Chem. Soc.* **2015**, *137*, 7079–7082.

(20) Wan, S.; Guo, J.; Kim, J.; Ihee, H.; Jiang, D. A Belt-Shaped, Blue Luminescent, and Semiconducting Covalent Organic Framework. *Angew. Chem., Int. Ed.* **2008**, *47*, 8826–8830.

(21) Xu, H.; Tao, S.; Jiang, D. Proton conduction in crystalline and porous covalent organic frameworks. *Nat. Mater.* **2016**, *15*, 722–726.

(22) Zhang, G.; Li, X.; Liao, Q.; Liu, Y.; Xi, K.; Huang, W.; Jia, X. Water-dispersible PEG-curcumin/amine-functionalized covalent organic framework nanocomposites as smart carriers for in vivo drug delivery. *Nat. Commun.* **2018**, *9*, 2785.

(23) Sun, Q.; Fu, C.-W.; Aguila, B.; Perman, J.; Wang, S.; Huang, H.- Y.; Xiao, F.-S.; Ma, S. Pore Environment Control and Enhanced Performance of Enzymes Infiltrated in Covalent Organic Frameworks. *J. Am. Chem. Soc.* **2018**, *140*, 984–992.

(24) Cote, A. P.; Benin, A. I.; Ockwig, N. W.; O’Keeffe, M.; Matzger, A. J.; Yaghi, O. M. Porous, crystalline, covalent organic frameworks. *Science* **2005**, *310*, 1166–1170.

(25) Yaghi, O. M.; Li, G.; Li, H. Selective binding and removal of guests in a microporous metal-organic framework. *Nature* **1995**, *378*, 703–706.

(26) Kondo, M.; Yoshitomi, T.; Seki, K.; Matsuzaka, H.; Kitagawa, S. Three-Dimensional Framework with Channeling Cavities for Small Molecules: {[M_2(4,4′-bpy)$_3$(NO_3)$_4$]·$x$$H_2O$}$_n$ (M = Co, Ni, Zn). *Angew. Chem. Int. Ed. Engl.* **1997**, *36*, 1725-1727.

(27) Yaghi, O. M. Reticular Chemistry–Construction, Properties, and Precision Reactions of Frameworks. *J. Am. Chem. Soc.* **2016**, *138*, 15507–15509.

(28) Yaghi, O. M.; O'Keeffe, M.; Ockwig, N. W.; Chae, H. K.; Eddaoudi, M.; Kim, J. Reticular synthesis and the design of new materials. *Nature* **2003**, *423*, 705–714.

(29) Yaghi, O. M. Reticular Chemistry: Molecular Precision in Infinite 2D and 3D. *Mol. Front. J.* **2019**, *3*, 66–83.

(30) O'Keeffe, M.; Peskov, M. A.; Ramsden, S. J.; Yaghi, O. M. The Reticular Chemistry Structure Resource (RCSR) Database of, and Symbols for, Crystal Nets. *Acc. Chem. Res.* **2008**, *41*, 1782–1789.

(31) O'Keeffe, M.; Eddaoudi, M.; Li, H.; Reineke, T. M.; Yaghi, O. M. Frameworks for Extended Solids: Geometrical Design Principles. *J. Solid State Chem.* **2000**, *152*, 3–20.

(32) Boyd, P. G.; Woo, T. K. A generalized method for constructing hypothetical nanoporous materials of any net topology from graph theory. *CrystEngComm.* **2016**, *18*, 3777–3792.

(33) Yaghi, O. M. The Reticular Chemist. *Nano Lett.* **2020**, *20*, 8432–8434.

(34) Kim, J.; Chen, B.; Reineke, T. M.; Li, H.; Eddaoudi, M.; Moler, D. B.; O'Keeffe, M.; Yaghi, O. M. Assembly of Metal-Organic Frameworks from Large Organic and Inorganic Secondary Building Units: New Examples and Simplifying Principles for Complex Structures. *J. Am. Chem. Soc.* **2001**, *123*, 8239–8247.

(35) Jin, F.; Lin, E.; Wang, T.; Geng, S.; Wang, T.; Liu, W.; Xiong, F.; Wang, Z.; Chen, Y.; Cheng, P.; Zhang, Z. Bottom-Up Synthesis of 8-Connected Three-Dimensional Covalent Organic Frameworks for Highly Efficient Ethylene/Ethane Separation. *J. Am. Chem. Soc.* **2022**, *144*, 5643−5652.

(36) Lyle, S. J.; Waller, P. J.; Yaghi, O. M. Covalent Organic Frameworks: Organic Chemistry Extended into Two and Three Dimensions. *Trends Chem.* **2019**, *1*, 172–184.

(37) Jiang, D. Covalent Organic Frameworks: An Amazing Chemistry Platform for Designing Polymers. *Chem.* **2020**, *6*, 2461–2483.

(38) Guan, X.; Fang, Q.; Yan, Y.; Qiu, S. Functional Regulation and Stability Engineering of Three-Dimensional Covalent Organic Frameworks. *Acc. Chem. Res.* **2022**, *55*, 1912–1927.

(39) El-Kaderi, H. M.; Hunt, J. R.; Mendoza-Cortés, J. L.; Côté, A. P.; Taylor, R. E.; O'Keeffe, M.; Yaghi, O. M. Designed synthesis of 3D covalent organic frameworks. *Science* **2007**, *316*, 268–272.

(40) Uribe-Romo, F. J.; Hunt, J. R.; Furukawa, H.; Klöck, C.; O'Keeffe, M.; Yaghi, O. M. A crystalline imine-linked 3-D porous covalent organic framework. *J. Am. Chem. Soc.* **2009**, *131*, 4570–4571.

(41) Lin, G.; Ding, H.; Yuan, D.; Wang, B.; Wang, C. A Pyrene-Based, Fluorescent Three-Dimensional Covalent Organic Framework. *J. Am. Chem. Soc.* **2016**, *138*, 3302–3305.

(42) Zhang, Y.; Duan, J.; Ma, D.; Li, P.; Li, S.; Li, H.; Zhou, J.; Ma, X.; Feng, X.; Wang, B. Three-Dimensional Anionic Cyclodextrin-Based Covalent Organic Frameworks. *Angew. Chem., Int. Ed.* **2017**, *56*, 16313–16317.

(43) Ma, T.; Kapustin, E. A.; Yin, S. X.; Liang, L.; Zhou, Z.; Niu, J.; Li, L. H.; Wang, Y.; Su, J.; Li, J.; Wang, X.; Wang, W. D.; Wang, W.; Sun, J.; Yaghi, O. M. Single-crystal x-ray diffraction structures of covalent organic frameworks. *Science* **2018**, *361*, 48–52.

(44) Xie, Y.; Li, J.; Lin, C.; Gui, B.; Ji, C.; Yuan, D.; Sun, J.; Wang, C. Tuning the Topology of Three-Dimensional Covalent Organic Frameworks via Steric Control: From pts to Unprecedented ljh. *J. Am. Chem. Soc.* **2021**, *143*, 7279–7284.

(45) Li, H.; Ding, J.; Guan, X.; Chen, F.; Li, C.; Zhu, L.; Xue, M.; Yuan, D.; Valtchev, V.; Yan, Y.; Qiu, S.; Fang, Q. Three-Dimensional Large-Pore Covalent Organic Framework with stp Topology. *J. Am. Chem. Soc.* **2020**, *142*, 13334–13338.

(46) Zhu, Q.; Wang, X.; Clowes, R.; Cui, P.; Chen, L.; Little, M. A.; Cooper, A. I. 3D Cage COFs: A Dynamic Three-Dimensional Covalent Organic Framework with High-Connectivity Organic Cage Nodes. *J. Am. Chem. Soc.* **2020**, *142*, 16842–16848.

(47) Li, H.; Chen, F.; Guan, X.; Li, J.; Li, C.; Tang, B.; Valtchev, V.; Yan, Y.; Qiu, S.; Fang, Q. Three-Dimensional Triptycene-Based Covalent Organic Frameworks with ceq or acs Topology. *J. Am. Chem. Soc.* **2021**, *143*, 2654–2659.

(48) Li, Z.; Sheng, L.; Wang, H.; Wang, X.; Li, M.; Xu, Y.; Cui, H.; Zhang, H.; Liang, H.; Xu, H.; He, X. Three-Dimensional Covalent Organic Framework with ceq Topology. *J. Am. Chem. Soc.* **2021**, *143*, 92–96.

(49) Yu, C.; Li, H.; Wang, Y.; Suo, J.; Guan, X.; Wang, R.; Valtchev, V.; Yan, Y.; Qiu, S.; Fang, Q. Three-Dimensional Triptycene-Functionalized Covalent Organic Frameworks with hea Net for Hydrogen Adsorption. *Angew. Chem. Int. Ed.* **2022**, *61*, e202117101.

(50) Li, Z.; Sheng, L.; Hsueh, C.; Wang, X.; Cui, H.; Gao, H.; Wu, Y.; Wang, J.; Tang, Y.; Xu, H.; He, X. Three-Dimensional Covalent Organic Frameworks with hea Topology. *Chem. Mater.* **2021**, *33*, 9618–9623.

(51) Martinez-Abadia, M.; Strutynski, K.; Lerma-Berlanga, B.; Stoppiello, C. T.; Khlobystov, A. N.; Marti-Gastaldo, C.; Saeki, A.; Melle-Franco, M.; Mateo-Alonso, A. π-Interpenetrated 3D Covalent Organic Frameworks from Distorted Polycyclic Aromatic Hydrocarbons. *Angew. Chem. Int. Ed.* **2021**, *60*, 9941–9946.

(52) Lan, Y.; Han, X.; Tong, M.; Huang, H.; Yang, Q.; Liu, D.; Zhao, X.; Zhong, C. Materials genomics methods for high-throughput construction of COFs and targeted synthesis. *Nat. Commun.* **2018**, *9*, 5274.

(53) Yahiaoui, O.; Fitch, A. N.; Hoffmann, F.; Fröba, M.; Thomas, A.; Roeser, J. 3D Anionic Silicate Covalent Organic Framework with srs Topology. *J. Am. Chem. Soc.* **2018**, *140*, 5330−5333.

(54) Nguyen, H. L.; Gropp, C.; Ma, Y.; Zhu, C.; Yaghi, O. M. 3D Covalent Organic Frameworks Selectively Crystallized through Conformational Design. *J. Am. Chem. Soc.* **2020**, *142*, 20335−20339.

(55) Kang, X.; Han, X.; Yuan, C.; Cheng, C.; Liu, Y.; Cui, Y. Reticular Synthesis of tbo Topology Covalent Organic Frameworks. *J. Am. Chem. Soc.* **2020**, *142*, 16346−16356.

(56) Wang, X.; Bahri, M.; Fu, Z.; Little, M. A.; Liu, L.; Niu, H.; Browning, N. D.; Chong, S. Y.; Chen, L.; Ward, J. W.; Cooper, A. I. A Cubic 3D Covalent Organic Framework with nbo Topology. *J. Am. Chem. Soc.* **2021**, *143*, 15011−15016.

(57) Shan, Z.; Wu, M.; Zhu, D.; Wu, X.; Zhang, K.; Verduzco, R.; Zhang, G. 3D Covalent Organic Frameworks with Interpenetrated pcb Topology Based on 8-Connected Cubic Nodes. *J. Am. Chem. Soc.* **2022**, *144*, 5728−5733.

(58) Jin, F.; Lin, E.; Wang, T.; Geng, S.; Wang, T.; Liu, W.; Xiong, F.; Wang, Z.; Chen, Y.; Cheng, P.; Zhang, Z. Bottom-Up Synthesis of 8-Connected Three-Dimensional Covalent Organic Frameworks for Highly Efficient Ethylene/Ethane Separation. *J. Am. Chem. Soc.* **2022**, *144*, 5643−5652.

(59) *Materials Studio* ver. 7.0; Accelrys Inc.: San Diego, CA.

(60) Maheshwari, M.; Ketkar, A. R.; Chauhan, B.; Patil, V. B.; Paradkar, A. R. Preparation and characterization of ibuprofen–cetyl alcohol beads by melt solidification technique: effect of variables. *Int. J. Pharm.* **2003**, *261*, 57–67.

(61) Varrassi, G.; Pergolizzi, J. V.; Dowling, P.; Paladini, A. Ibuprofen Safety at the Golden Anniversary: Are all NSAIDs the Same? A Narrative Review. *Adv. Ther.* **2020**, *37*, 61–82.

(62) Dawood, M. Y. Ibuprofen and Dysmenorrhea. *Am. J. Med.* **1984**, *77*, 87–94.

(63) Vallet-Regi, M.; Rámila, A.; del Real, R. P.; Pérez-Pariente, J. A New Property of MCM-41: Drug Delivery System. *Chem. Mater.* **2001**, *13*, 308–311.

(64) Fang, Q.; Wang, J.; Gu, S.; Kaspar, R. B.; Zhuang, Z.; Zheng, J.; Guo, H.; Qiu, S.; Yan, Y. 3D Porous Crystalline Polyimide Covalent Organic Frameworks for Drug Delivery. *J. Am. Chem. Soc.* **2015**, *137*, 8352−8355.

(65) Christensen, S.; Paluch, E.; Jayawardena, S.; Daniels, S.; Meeves, S. Analgesic Efficacy of a New Immediate-Release/Extended-Release Formulation of Ibuprofen: Results From Single- and Multiple-Dose Postsurgical Dental Pain Studies. *Clin. Pharmacol. Drug Dev.* **2017**, *6*, 302–312.

(66) Nicholson, B. Benefits of Extended-Release Opioid Analgesic Formulations in the Treatment of Chronic Pain. *Pain Pract.* **2009**, *9*, 71–81.

Table of Contents